Materials Advances

ROYAL SOCIETY OF CHEMISTRY

HIGHLIGHT

View Article Online
View Journal | View Issue

Cite this: *Mater. Adv.*, 2023, 4, 2770

Synthesis of novel mesoporous silica nanoparticles functionalized with succinic dihydrazone Schiff-base metal complexes and a study of their biological activities

Leila Tahmasbi, *[a] Tahereh Sedaghat,[a] Hossein Motamedi[bc] and Mohammad kooti[a]

Received 11th February 2023,
Accepted 5th June 2023

DOI: 10.1039/d3ma00066d

rsc.li/materials-advances

For the first time, functionalized mesoporous silica nanoparticles (MSNs) with dinuclear Schiff-base complexes were synthesized as attractive organic–inorganic hybrids and their capability investigated for loading antibiotic drugs and immobilization of enzymes. 2D-hexagonal MCM-41 nanoparticles were synthesized by a sol–gel method and amino propyl trimethoxy silane (APTMS) anchored on the surface of the MSNs as a linker. MSN-APS nanoparticles were coordinated with dihydrazone Schiff-base complexes of copper(II) and nickel(II) by the nitrogen atom of APS for making MSN-APS-Cu_2L and MSN-APS-Ni_2L hybrids, respectively (L is the Schiff-base ligand). These novel mesoporous silica nanoparticles were characterized by various techniques, such as FT-IR, LA-XRD, FE-SEM, TEM, EDX, BET and TGA. The results show that the synthesized hybrids have high potential for loading gentamicin and immobilizing enzymes such as DNase, coagulase and α-amylase.

Introduction

Mesoporous materials with a pore size of 2–50 nm have attracted the attention of various scientists since their discovery in 1992.[1–3] About a decade later, other mesoporous silica nanoparticles were also synthesized and studied.[4] The remarkable characteristics of these new materials are: controllable pore and particle size, stable suspension for long periods, high surface area, mechanical and chemical stability and low toxicity.[4–7] Mesoporous silica nanoparticles (MSNs) are divided into five categories: 2D-hexagonal MCM-41 (MCM-41s), swollen pore MCM-41 (SMCM-41s), hollow mesoporous nanoparticles (HNPs), rod-like MCM-41 (RMCM-41s) and radial mesoporous silica nanoparticles (RNPs).[8–12] Among them, MCM-41 with a particle size of 50–200 nm has many interesting features, such as biocompatibility, stability, good interactions with many drugs for use as antibacterial agents, ease of functionalization and high surface area.[13–16] In recent years, organic groups or inorganic compounds (in the form of metal complexes) were grafted on the surface of MSNs. Metal complexes supported on MSNs are utilized in various fields, such as catalysis, drug delivery, fluorescence, pollutant removal, photodynamic therapy and tooth bleaching, as well as enzyme immobilization.[9,17–28] Metal complexes of Ni^{2+}, Co^{2+} and Cu^{2+} have been grafted on carbon nanotubes, quantum dots and various nanoparticles, such as Au, Fe_2O_3 and SiO_2.[29–32] Grafting of metal complexes on nanoparticles has resulted in an increase in the stability and lifetimes of the enzymes.[33] Among the ligands and complexes, bis-acyl-hydrazones and their metal complexes have shown excellent properties for catalytic, anticancer, antibacterial and antifungal activities.[34–51] Therefore, with regard to the importance of MSNs, bis-acyl-hydrazones and their complexes, in this research work we report the synthesis of new organic–inorganic hybrids and their characterization, and an investigation of the capability of these compounds to show biological activities. 3-(Aminopropyl) triethoxysilane (APTMS) was functionalized on MSN and grafted onto bis-acyl-hydrazone Schiff-base complexes of Ni^{2+} and Cu^{2+}. These novel hybrids, including binuclear metal complexes grafted on the surface of MSN through linkers, have exhibited attractive properties, such as high surface area, biocompatibility, thermal and mechanical stability, and a high number of active sites (metallic centers) for stabilizing enzymes and loading therapeutic agents. The ability of the new hybrids to load gentamicin, and their antibacterial activities as well as the immobilization of α-amylase, DNase and coagulase enzymes were investigated.

[a] *Department of Chemistry, College of Sciences, Shahid Chamran University of Ahvaz, Ahvaz, Iran. E-mail: tahmasbi_l@yahoo.com*
[b] *Department of Biology, College of Sciences, Shahid Chamran University of Ahvaz, Ahvaz, Iran*
[c] *Biotechnology and Biological Science Research Center, Shahid Chamran University of Ahvaz, Ahvaz, Iran*

Experimental

Synthesis of bis(2-hydroxybenzaldehyde) succinic dihydrazone(H_4L)

1 mmol (0.146 g) of succinic dihydrazide was dissolved in 25 mL of absolute ethanol in a flask and heated and stirred for 30 min. Then 0.3 mL (2 mmol) of salicylaldehyde was slowly added to the solution. The mixture was refluxed for 3 h. The obtained white precipitate was filtered, washed with absolute ethanol and dried in an oven at 80 °C for 5 h. This compound was characterized by FT-IR.

Synthesis of bis-acyl-hydrazone complexes Cu_2L and Ni_2L

A mixture of 0.28 mmol (0.1 g) of H_4L and 25 mL of absolute ethanol was added to a flask and heated and stirred for 30 min. Then 0.56 mmol of acetate salts of Cu^{2+} and Ni^{2+} was dissolved in ethanol. The solution of salts was added to the ligand solution to obtain Cu_2L and Ni_2L. The mixtures were refluxed for 3 h. The obtained green (Cu_2L) and brown (Ni_2L) precipitates were filtered, washed with absolute ethanol and dried at room temperature. These compounds were characterized with FT-IR.

Synthesis of MSNs and MSN-APS

1 g of CTAB was dissolved in 480 mL of deionized water and stirred vigorously. Then 3.5 mL of 2M NaOH was added to this solution and it was heated at 80 °C for 4 h. 5 mL of TEOS was added dropwise into the solution and stirred for 2 h at 80 °C to form a white gel. This white gel was collected, washed several times with deionized water and dried at 80 °C in an oven overnight. The obtained MNS product was dispersed in acidic ethanol and refluxed for 24 h. To prepare MSN-APS, 0.1 g of pre-synthesized MSN was dispersed in 80 mL of ethanol, and 1 mL of 3-aminopropyl triethoxysilane (APTMS) was slowly added to this suspension and stirred. This mixture was refluxed for 3 h. Then it was filtered, thoroughly washed with ethanol and dried in an oven at 80 °C for 12 h. The MSNs were characterized by FT-IR, FE-SEM, EDX, LA-XRD, BET.

Synthesis MSN-APS-Cu_2L and MSN-APS-Ni_2L

0.1 g of MSN-APS was dispersed in 20 mL of absolute ethanol and stirred for 30 min. A solution containing 0.1 mmol of Schiff-base complexes Cu_2L (0.044 g) or Ni_2L (0.045 g) was sonicated in 10 mL of absolute ethanol for 10 min and gradually added to the MSN-APS solution. The mixture was stirred at room temperature for 12 h. The nanoparticles were filtered and washed several times with ethanol until the solution under filtration became colorless. The collected products were dried in an oven at 80 °C for 24 h. Different stages of the synthesis of hybrid mesoporous silica nanoparticles are shown in Fig. 1. MSN-APS-Cu_2L and MSN-APS-Ni_2L nanoparticles were characterized by FT-IR, FE-SEM, TEM, EDX, LA-XRD, BET and TGA techniques.

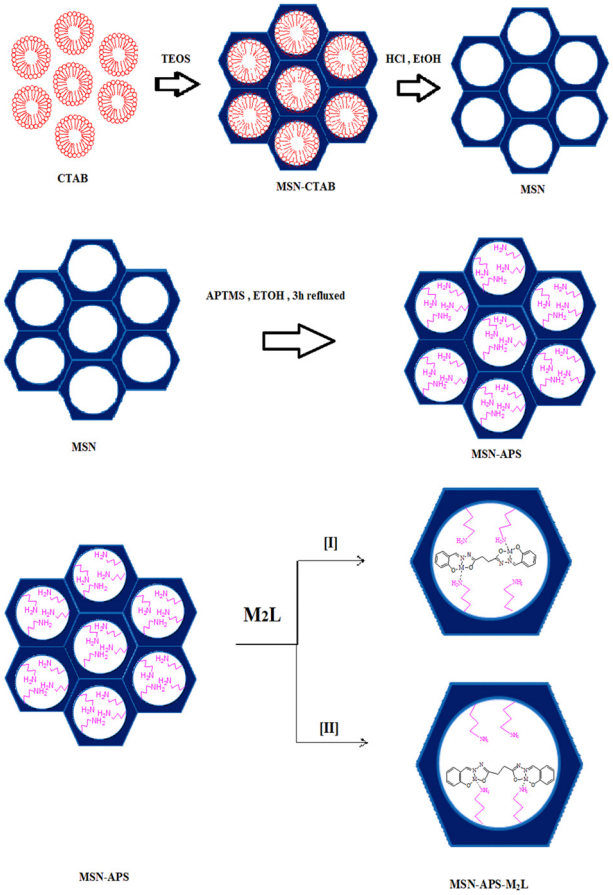

Fig. 1 Schematic of synthesized mesoporous silica nanoparticles.

Biological experiments

Several microbial tests and enzyme immobilization were accomplished in this research work. In the first part the intrinsic antibacterial activity of MSN-APS-Cu_2L and MSN-APS-Ni_2L was registered against *Escherichia coli* (ATCC 25922) and *Staphylococcus aureus* (ATCC 6538) bacteria in Mueller–Hinton broth culture medium. 100 μL of bacterial suspension that had grown until 0.5 McFarland turbidity was added to 20 mg of each compound in 5 mL of Mueller–Hinton broth and incubated at 37 °C (Merck, Germany). Simultaneously, a culture was prepared from each bacterial species without nanoparticles and a culture was prepared with nanoparticles without bacterial inoculation. The optical density of the different samples was measured with an ELISA microplate reader at 665 nm over 24 h. In the second part the loading of MSN, MSN-APS, MSN-APS-Cu_2L and MSN-APS-Ni_2L nanoparticles was examined with gentamicin antibiotic and their inhibitory activities were investigated against four bacterial species. For this test, 10 mg of gentamicin was dissolved in 1 mL of MQ water and added to 20 mg of nanoparticles. For proper loading, samples were kept in an incubator for 24 h at 37 °C. After three washings of the nanoparticles with MQ-water, the antibacterial activity of the nanocomposites and Gen@nanocomposites was investigated against Gram-positive bacteria, *i.e.*, *Staphylococcus aureus*

(ATCC 6538) and *Bacillus subtilis* (ATCC 6633), and two Gram-negative species, *i.e.*, *Escherichia coli* (ATCC 25922) and *Pseudomonas aeruginosa* (ATCC 9027) according to the standard Kirby–Bauer disc diffusion method recommended by CLSI guidelines. In the third part, the capacity of enzyme immobilization of these new organic–inorganic hybrids was studied. Three enzymes were used for this examination: α-amylase (Sigma Company), coagulase and DNase (from *S. aureus*). The concentration of α-amylase was 2 mg in 1 mL of PBS and those of coagulase and DNase were 1 mL with respect to 20 mg of each composite. In case of α-amylase, a solution of pure enzyme (2 mg mL^{-1} PBS) was prepared and 20 mg of each nanocomposite was added to 1 mL of this solution and incubated at 37 °C for 24 h. These nanoparticles were then washed three times with PBS and dispersed in 500 μL sterile distilled water. Finally, the enzyme loadings on these compounds were evaluated through culturing on starch agar, a plasma coagulation test and clear halo zone formation on DNase agar.

Results and discussion

FT-IR spectroscopy

The FT-IR spectra of H_4L, Cu_2L, Ni_2L, MSN-APS-Cu_2L and MSN-APS-Ni_2L are shown in Fig. 2. Information about the FT-IR spectra of MSN and MSN-APS was reported in our earlier article.[52,53] In the FT-IR spectra of H_4L appeared bands of –OH (3428 cm^{-1}), –NH (3201 cm^{-1}), aromatic –CH (3054 cm^{-1}) and aliphatic –CH (2857–2928 cm^{-1}). Also the bands of C=O and C=N were observed at 1662 cm^{-1} and 1622 cm^{-1}.[54,55] In the IR spectra of binuclear Schiff-base complexes Cu_2L and Ni_2L, carbonyl bands had vanished and the imine groups had decreased to 1618 cm^{-1} and 1606 cm^{-1}, respectively, because of coordination of the imine of the ligand to transition metals ions. In the Cu_2L spectra, the bands at 491 cm^{-1} and 597 cm^{-1} were related to the vibrations of Cu–N and Cu–O. The vibrations for Ni_2L were observed at 525 cm^{-1} and (Ni–N) 616 cm^{-1} (Ni–O). The FT-IR spectra of organic–inorganic hybrids of MSN-APS-Cu_2L and MSN-APS-Ni_2L showed that the MSN-APS and binuclear Schiff-base complexes were grafted together, because the bands of the silanol groups (Si–O–Si) at 1085, 802, 465 cm^{-1} and the imine of bis-acyl-hydrazone complexes were seen for MSN-APS-Cu_2L and MSN-APS-Ni_2L.

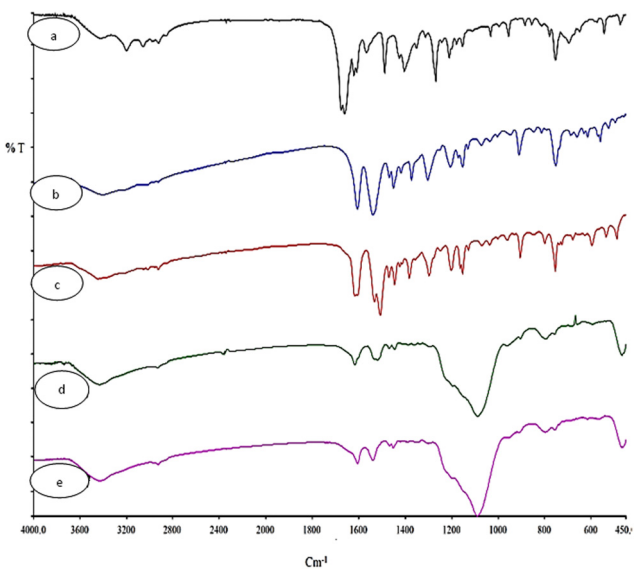

Fig. 2 FT-IR spectra of synthesized nanohybrids (a) L, (b) Ni_2L, (c) Cu_2L, (d) MSN-APS-Cu_2L and (e) MSN-APS-Ni_2L.

FE-SEM and TEM

As shown in the FE-SEM images, MSN-APS-Cu_2L and MSN-APS-Ni_2L had monotonous spherical morphology and their mean diameter was estimated as approximately less than 100 nm by ImageJ software (Fig. 3(a)–(c)). Also, the spherical morphology of the initial MSN was preserved for these organic–inorganic nanohybrids, which demonstrated that the Schiff-base complexes had settled on the surface of the nanoparticles or on the surface of channel-like pores. Mesoporous channels were clearly observed in the TEM images of MSN-Cu_2L, with a hexagonal ordered arrangement. Obvious channel-like pores parallel to each other can be seen (Fig. 4).

EDX

The elemental content of MSN, MSN-APS-Cu_2L and MSN-APS-Ni_2L was investigated by using energy dispersed X-ray (EDX) spectroscopy. The EDX spectral patterns of the nanoparticles are shown in Fig. 5: MSN (Si: 43.64% and O: 56.36%), MSN-APS-Cu_2L (Si: 14.61%, O: 48.71%, N: 7.62%, C: 28.50% and Cu: 1.26%) and MSN-APS-Ni_2L (Si: 16.91%, O: 41.41%, N: 6.13%, C: 35.14% and Ni: 0.40%). The EDX results indicate the presence of the expected elements in the structure of the nanoparticles and prove their formation.

XRD

The low-angle powder X-ray diffraction in the $0.8^\circ < 2\theta < 10^\circ$ range for MSN-APS-Cu_2L and MSN-APS-Ni_2L can be seen in Fig. 6. In our previous work, the patterns for MSNs had four reflection peaks with different intensities that indicate Bragg peaks by indexing planes (100), (110), (200) and (210) at 2θ = 2.27°, 3.88°, 4.50°, and 5.94°, respectively.[52] This XRD pattern exhibited a hexagonal arrangement of pores and the 2D-MCM-41 structure of the nanoparticles.[56] The XRD patterns of MSN-APS-Cu_2L and MSN-APS-Ni_2L compared with MSN show two peaks at 2θ = 2.01°and 2.11° (high intensity) and at 4.2°and 4.08° (low intensity), while the other peaks had vanished because the mesoporous channels were filled with binuclear Schiff-base complexes as well as a decreased order of mesopores (Fig. 6(a) and (b)). The position of index peak (100) was used to calculate the interplanar spacings d_{100} for the materials. The d_{100} values were used to calculate the distances between pore centers a_0 $\left(a_0 = \frac{2d_{100}}{\sqrt{3}}\right)$. The calculated values of a_0 for MSN, MSN-APS-Cu_2L and MSN-APS-Ni_2L are 4.48 nm, 5 nm and 4.82 nm, respectively. The values of FWHM were

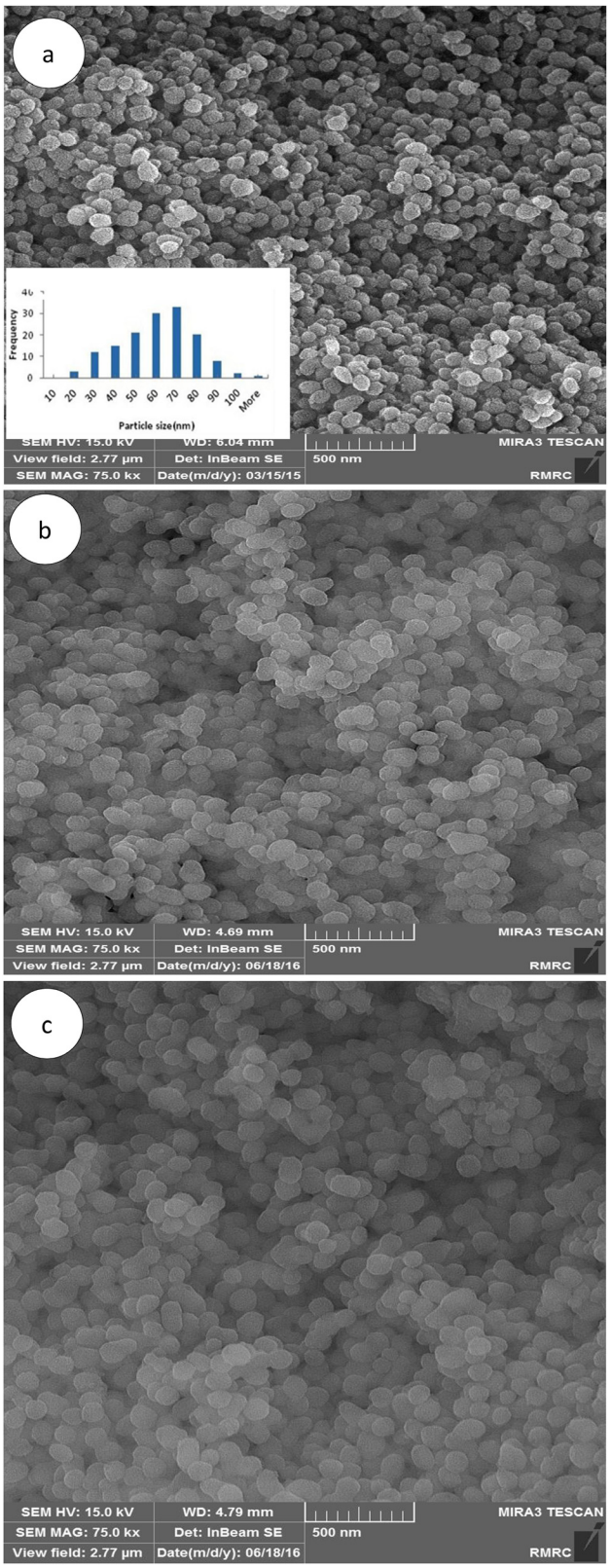

Fig. 3 FE-SEM images of the MSNs and functionalized MSNs: (a) MSN, (b) MSN-APS-Cu_2L and (c) MSN-APS-Ni_2L.

extracted from the curves and used to calculate the particle size of the crystallite (D). According to the Debye–Scherrer equation,

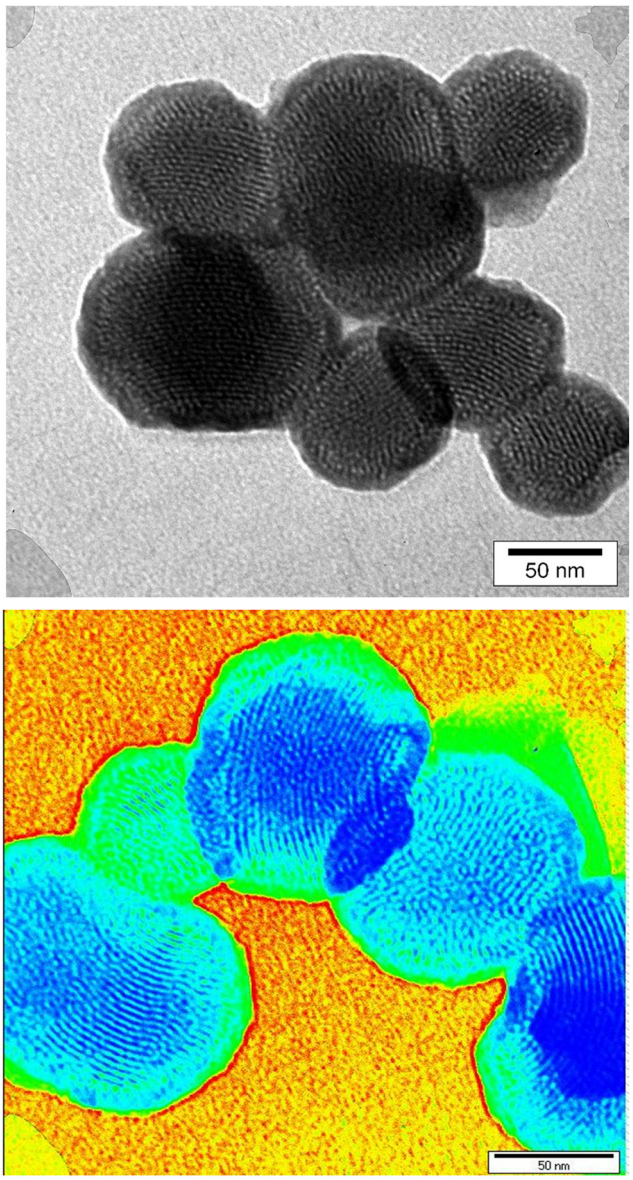

Fig. 4 TEM images of MSN-APS-Cu_2L.

the D value for MSN-APS-Cu_2L is 23.89 nm and that for MSN-APS-Ni_2L is 24.31 nm.

TGA

According to the thermogravimetric curves of MSN-APS-Cu_2L and MSN-APS-Ni_2L two main weight loss steps were observed from 25 °C to 800 °C at a heating rate of 10 °C min^{-1} (Fig. 7). The first step of decreasing weight was related to loss of physical water or organic solvents on the surface. The second step (22% loss weight) was attributed to the decomposition of the organic linker and the organic parts of binuclear Schiff-base complexes on MSNs from 250 to 450 °C. The amount of binuclear complexes grafted on MSN was estimated as 0.53 mmol g^{-1}. The residual mass up to 450 °C is related to the inorganic parts, including metals and silica components.

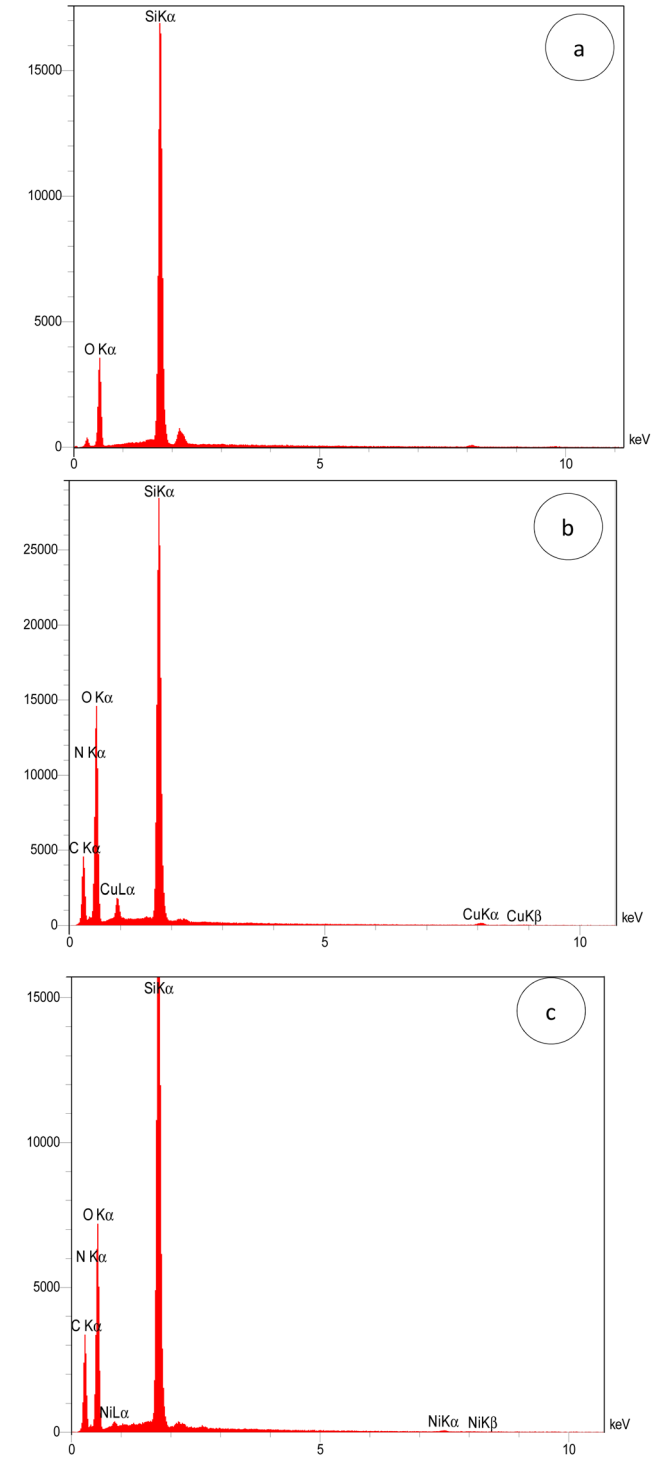

Fig. 5 EDX patterns of (a) MSN, (b) MSN-APS-Cu_2L and (c) MSN-APS-Ni_2L.

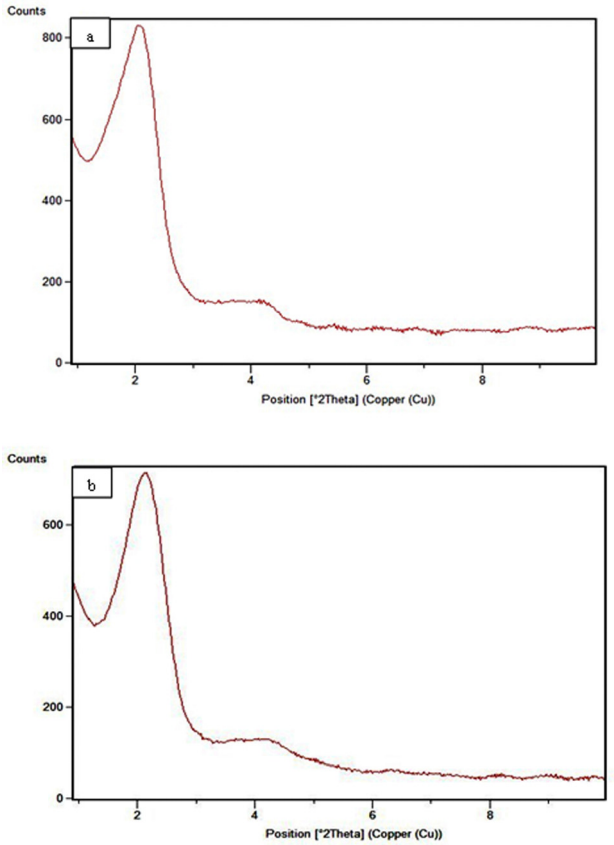

Fig. 6 Low-angle XRD patterns: (a) MSN-APS-Cu_2L and (b) MSN-APS-Ni_2L.

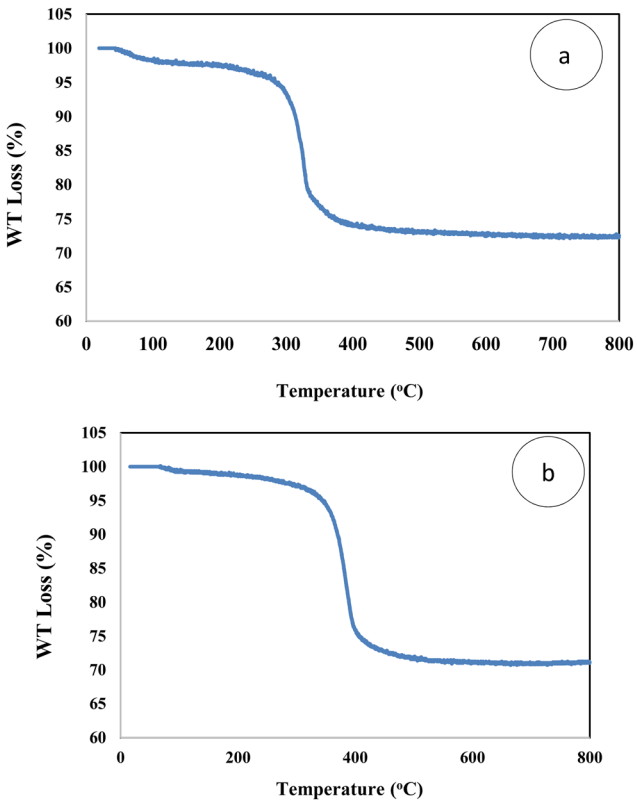

Fig. 7 TGA curves of (a) MSN-APS-Cu_2L and (b) MSN-APS-Ni_2L.

BET

The isotherms of N_2 absorption–desorption for MSN, MSN-APS-Cu_2L and MSN-APS-Ni_2L are displayed in Fig. 8. The patterns of these nanoparticles exhibit type IV isotherms, as expected for mesoporous silica with cylindrical and very uniform pores. The sharp rise at a relative pressure of 0.2–0.4 showed that the pores of the nanoparticles are very narrow. The specific surface area

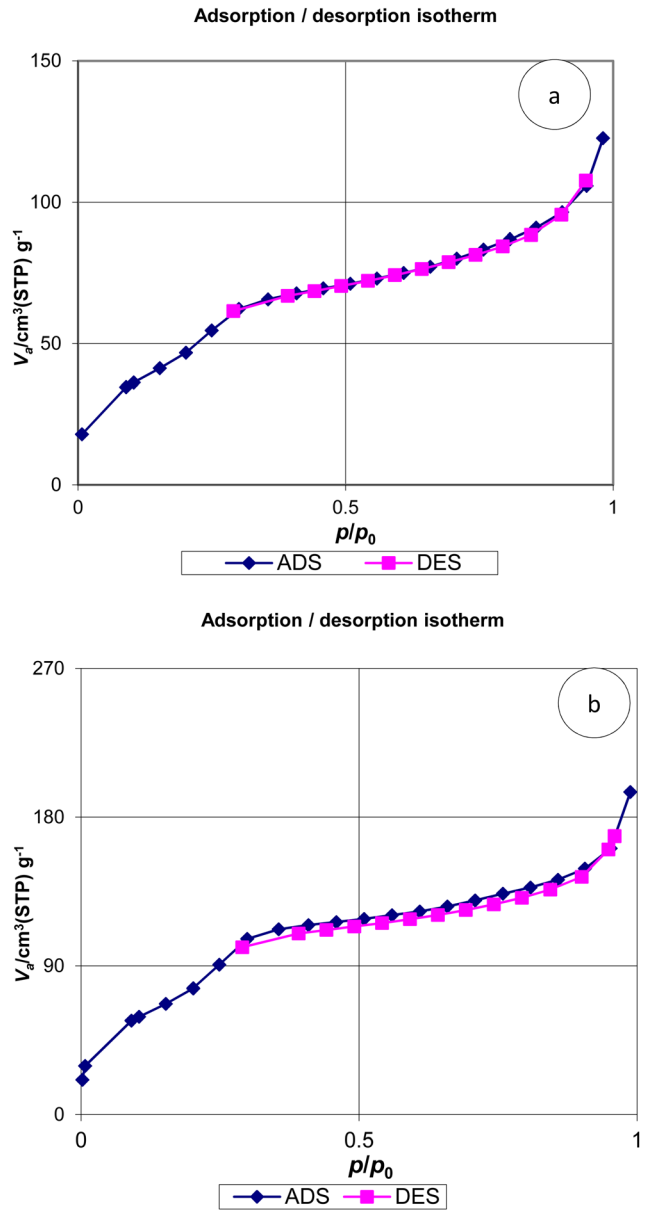

Fig. 8 N_2 adsorption–desorption isotherms of (a) MSN-APS-Cu_2L and (b) MSN-APS-Ni_2L.

(s), pore volume (v_p) and pore radius (r_p) of the nanoparticles were calculated by the BET and BJH methods. The data obtained from these methods for MSN-APS-Cu_2L were s = 179.34 $m^2\ g^{-1}$, v_p = 0.174 $cm^3\ g^{-1}$, and r_p = 1.21 nm and for MSN-APS-Ni_2L were s = 305.6 $m^2\ g^{-1}$, v_p = 0.278 $cm^3\ g^{-1}$, and r_p = 1.21 nm. The values of v_p and r_p decreased compared to those of MSN (s = 789 $m^2\ g^{-1}$, v_p = 0.782 $cm^3\ g^{-1}$, r_p = 1.21 nm) because of the anchoring of binuclear Schiff-base complexes on the surface of the pores of MSNs.

Biological activity

In this work, the new organic–inorganic hybrids were studied for their antibacterial activity, gentamicin loading potential and enzyme immobilization. Investigation of the growth of treated

Table 1 Antibacterial effect of synthesized nanohybrids

Compounds	Inhibition zone (mm)			
	S. aureus	*B. subtilis*	*E. coli*	*P. aeruginosa*
MSN	10[a]	0	0	10[a]
MSN-APS	10[a]	0	0	10[a]
MSN-APS-Cu_2L	10[b]	13[b]	0	13[a]
MSN-APS-Ni_2L	10[a]	10[a]	0	10[a]
MSN@Gen	10[b]	9[b]	10[b]	8[b]
MSN-APS@Gen	13[b], 15[a]	15[b]	16[b]	10[b]
MSN-APS-Cu_2L@Gen	20[b]	19[b]	20[b]	15[b]
MSN-APS-Ni_2L@Gen	15[b]	17[b]	20[b]	18[b]

[a] Inhibitory effect. [b] Bactericidal effect.

bacteria showed that MSN-APS-Cu_2L had bactericidal effects against *S. aureus* and *B. subtilis*. The effect of gentamicin-loaded mesoporous nanoparticles was discovered by a disc diffusion method. The results of this assay for nanoparticles alone and nanoparticles@Gen are presented in Table 1. MSN, MSN-APS-Cu_2L and MSN-APS-Ni_2L loaded gentamicin had more antibacterial activity than MSN or MSN-APS because, due to their bis-hydrazone groups and active metal ion centers, they have good interaction with the $-NH_2$ and –OH groups of gentamicin.[56] The results of the inhibition zone of composites and nanoparticles@Gen against *S. aureus*, *B. subtilis*, *E. coli* and *P.aeruginosa* are presented in Table 1 and Fig. 9 shows the effect of antibacterial activity of nanohybrids@Gen against *B. subtilis* and its comparison with MSN@Gen and MSN-APS@Gen. The results of enzyme immobilization for these compounds are presented in Tables 2 and 3. MSN-APS-Cu_2L and MSN-APS-Ni_2L showed glorious potential for immobilization of coagulase, DNase and α-amylase. Fig. 10, for example, shows a large clear zone around MSN-APS-Ni_2L@Am on starch agar, which means efficient immobilization of amylase and its diffusion in the culture medium. Also, coagulase-loaded MSN-APS-Cu_2L and MSN-APS-Ni_2L nanoparticles caused plasma clot formation over 1–2 h following addition to plasma. The good loading and stabilization of these enzymes on MSN-APS-Cu_2L and MSN-APS-Ni_2L were due to the interaction of the $-NH_2$ and $-COO^-$

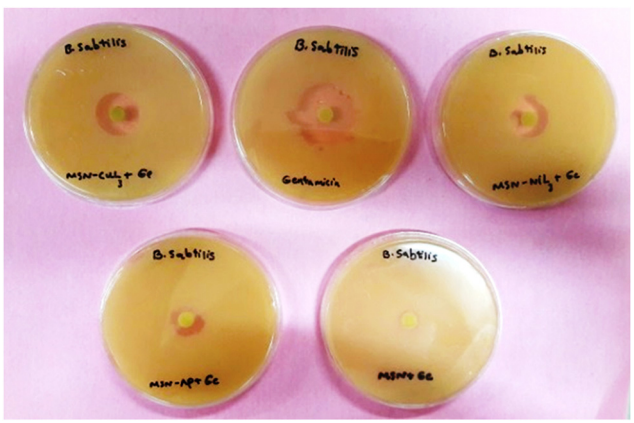

Fig. 9 Comparison of the antibacterial effects of MSN-APS-Ni_2L@Gen (top right), MSN-APS-Cu_2L (top left), gentamicin (top middle), MSN@Gen (bottom right) and MSN-APS@Gen (bottom left).

Table 2 The effect of loading of coagulase enzyme

hour	MSN@Coag	MSN-APS@Coag	MSN-APS-Cu_2L@Coag	MSN-APS-Ni_2L@Coag
1–2	–	–	+	+
18–24	+	+	+	+

Table 3 The effect of loading DNase enzyme

	MSN@Am	MSN-APS@Am	MSN-APS-Cu_2L@Am	MSN-APS-Ni_2L@Am
Effect zone	0	0	47	43

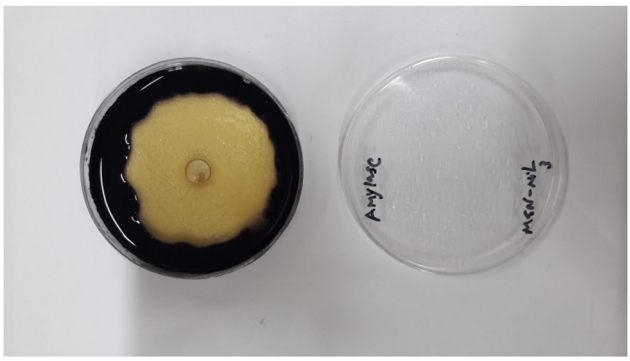

Fig. 10 Effect zone of MSN-APS-Ni_2L@Am.

groups of the enzymes with the empty coordination sites of metal complexes on MSN.[56–62] These hybrid nanoparticles also had greater effects as the bishydrazone Schiff-base ligands and binuclear complexes efficiently increased enzyme immobilization on MSN. Fig. 11–14 show that new MSNs functionalized by metal dinuclear compounds had a killing effect against *E. coli* and *S. aureus* bacteria in Mueller–Hinton broth. All these

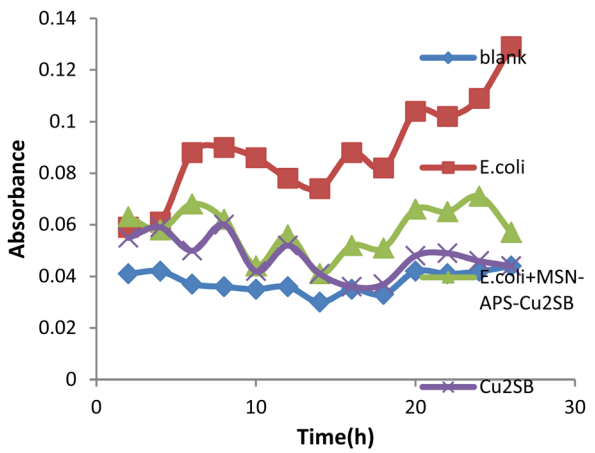

Fig. 11 Antibacterial activity of MSN-APS-Cu_2L against *E. coli* in Mueller–Hinton broth medium.

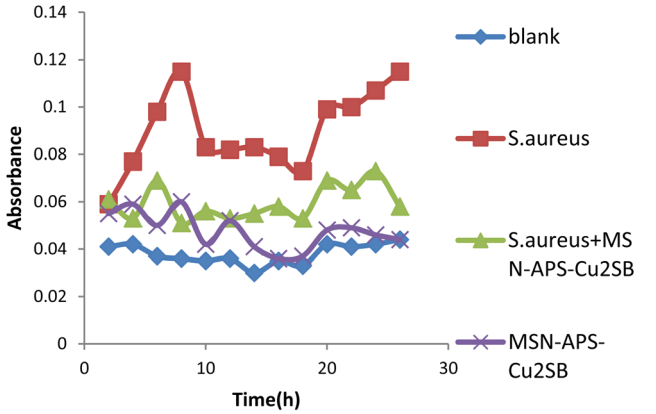

Fig. 12 Antibacterial activity of MSN-APS-Cu_2L against *S. aureus* in Mueller–Hinton broth medium.

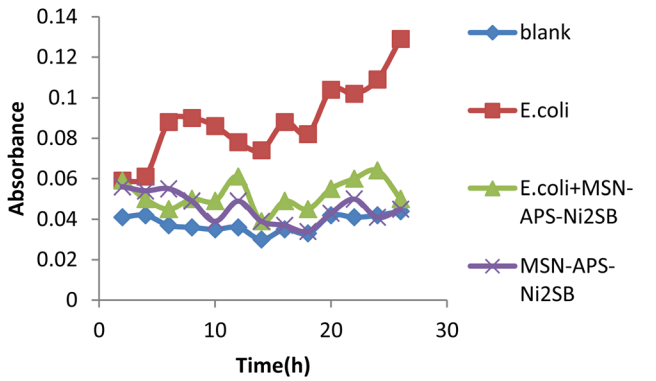

Fig. 13 Antibacterial activity of MSN-APS-Ni_2L against *E.coli* in Mueller–Hinton broth medium.

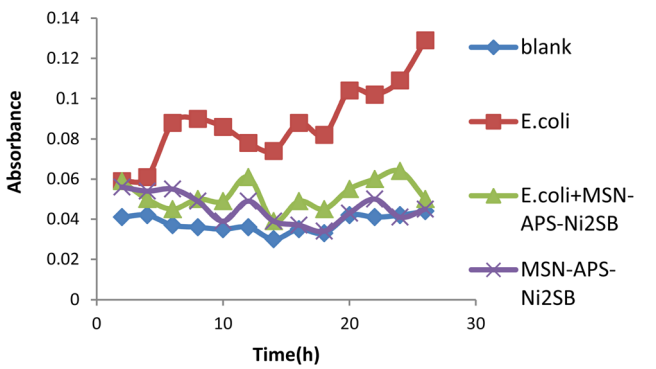

Fig. 14 Antibacterial activity of MSN-APS-Ni_2L against *S. aureus* in Mueller–Hinton broth medium.

microbial tests determined the importance and good potential applications of these new hybrids of MSNs.

Conclusions

New mesoporous silica nanoparticles with universal formulae MSN-APS-Cu_2L and MSN-APS-Ni_2L were synthesized by a

grafting method with success. These mesoporous silica nanoparticles are made from three important parts: MCM-41 nanoparticles, APTMS (linker) and Cu_2L and Ni_2L (binuclear Schiff-base complexes). These novel functionalized MSNs with dihydrazone complexes of Cu^{2+} and Ni^{2+} had interesting properties, such as keeping the particle sizes of the initial support, having a high surface area, suitable pore size, and metallic active sites for interaction with gentamicin antibiotic and DNase, coagulase and α-amylase enzymes. The antibacterial activity of MSN-APS-Cu_2L and MSN-APS-Ni_2L showed a bactericidal effect against *E. coli* and *S. aureus*. These compounds carried gentamicin antibiotic well and compared to MSN and MSN-APS showed better operation of loaded gentamicin. The results of enzyme immobilization showed that these two novel nanoparticles also stabilized DNase, coagulase and α-amylase.

Conflicts of interest

There are no conflicts to declare.

Acknowledgements

Support of this work by Shahid Chamran University of Ahvaz, Ahvaz, Iran (Grant No. 1395) is gratefully acknowledged.

Notes and references

1 C. Kresge, *et al.*, Ordered mesoporous molecular sieves synthesized by a liquid-crystal template mechanism, *Nature*, 1992, **359**(6397), 710–712.
2 C. T. Kresge and W. J. Roth, The discovery of mesoporous molecular sieves from the twenty year perspective, *Chem. Soc. Rev.*, 2013, **42**(9), 3663–3670.
3 N. Pal and A. Bhaumik, Soft templating strategies for the synthesis of mesoporous materials: Inorganic, organic–inorganic hybrid and purely organic solids, *Adv. Colloid Interface Sci.*, 2013, **189**, 21–41.
4 L. Yuan, *et al.*, Preparation of pH-responsive mesoporous silica nanoparticles and their application in controlled drug delivery, *J. Phys. Chem. C*, 2011, **115**(20), 9926–9932.
5 Z. Zou, *et al.*, Natural gelatin capped mesoporous silica nanoparticles for intracellular acid-triggered drug delivery, *Langmuir*, 2013, **29**(41), 12804–12810.
6 Y.-S. Lin and C. L. Haynes, Impacts of mesoporous silica nanoparticle size, pore ordering, and pore integrity on hemolytic activity, *J. Am. Chem. Soc.*, 2010, **132**(13), 4834–4842.
7 L. Minati, *et al.*, pH-activated doxorubicin release from polyelectrolyte complex layer coated mesoporous silica nanoparticles, *Microporous Mesoporous Mater.*, 2013, **180**, 86–91.
8 J. Lu, *et al.*, Biocompatibility, biodistribution, and drug-delivery efficiency of mesoporous silica nanoparticles for cancer therapy in animals, *Small*, 2010, **6**(16), 1794–1805.
9 I. I. Slowing, B. G. Trewyn and V. S.-Y. Lin, Mesoporous silica nanoparticles for intracellular delivery of membrane-impermeable proteins, *J. Am. Chem. Soc.*, 2007, **129**(28), 8845–8849.
10 L. Du, *et al.*, Controlled-access hollow mechanized silica nanocontainers, *J. Am. Chem. Soc.*, 2009, **131**(42), 15136–15142.
11 S. Yang, *et al.*, On the origin of helical mesostructures, *J. Am. Chem. Soc.*, 2006, **128**(32), 10460–10466.
12 Z. Li, *et al.*, Measurement of uptake and release capacities of mesoporous silica nanoparticles enabled by nanovalve gates, *J. Phys. Chem. C*, 2011, **115**(40), 19496–19506.
13 Y. Tian, *et al.*, Facile, one-pot synthesis, and antibacterial activity of mesoporous silica nanoparticles decorated with well-dispersed silver nanoparticles, *ACS Appl. Mater. Interfaces*, 2014, **6**(15), 12038–12045.
14 Z. Li, *et al.*, Mesoporous silica nanoparticles in biomedical applications, *Chem. Soc. Rev.*, 2012, **41**(7), 2590–2605.
15 G. Qi, *et al.*, Vancomycin-modified mesoporous silica nanoparticles for selective recognition and killing of pathogenic Gram-positive bacteria over macrophage-like cells, *ACS Appl. Mater. Interfaces*, 2013, **5**(21), 10874–10881.
16 D. Tarn, *et al.*, Mesoporous silica nanoparticle nanocarriers: biofunctionality and biocompatibility, *Acc. Chem. Res.*, 2013, **46**(3), 792–801.
17 C.-C. Liu, *et al.*, A room temperature catalyst for toluene aliphatic C–H bond oxidation: Tripodal tridentate copper complex immobilized in mesoporous silica, *J. Catal.*, 2015, **322**, 139–151.
18 Y. Yang, *et al.*, Oxovanadium (IV) and dioxomolybdenum (VI) salen complexes tethered onto amino-functionalized SBA-15 for the epoxidation of cyclooctene, *Solid State Sci.*, 2011, **13**(11), 1938–1942.
19 L. Yuan, *et al.*, Mechanistic study of the covalent loading of paclitaxel via disulfide linkers for controlled drug release, *Langmuir*, 2013, **29**(2), 734–743.
20 J. Gu, *et al.*, One-pot synthesis of mesoporous silica nanocarriers with tunable particle sizes and pendent carboxylic groups for cisplatin delivery, *Langmuir*, 2012, **29**(1), 403–410.
21 D. Zhang, *et al.*, Synthesis and characterization of novel lanthanide (III) complexes-functionalized mesoporous silica nanoparticles as fluorescent nanomaterials, *J. Phys. Chem. C*, 2010, **114**(29), 12505–12510.
22 Y. Yang, *et al.*, Heterogenization of functionalized Cu(II) and VO (IV) Schiff base complexes by direct immobilization onto amino-modified SBA-15: Styrene oxidation catalysts with enhanced reactivity, *Appl. Catal., A*, 2010, **381**(1), 274–281.
23 J. S. Valenstein, *et al.*, Functional mesoporous silica nanoparticles for the selective sequestration of free fatty acids from microalgal oil, *ACS Appl. Mater. Interfaces*, 2012, **4**(2), 1003–1009.
24 C. Argyo, *et al.*, Multifunctional mesoporous silica nanoparticles as a universal platform for drug delivery, *Chem. Mater.*, 2013, **26**(1), 435–451.
25 Z. Tao, *et al.*, Mesoporous silica microparticles enhance the cytotoxicity of anticancer platinum drugs, *ACS Nano*, 2010, **4**(2), 789–794.

26 M. Frasconi, *et al.*, Photoexpulsion of surface-grafted ruthenium complexes and subsequent release of cytotoxic cargos to cancer cells from mesoporous silica nanoparticles, *J. Am. Chem. Soc.*, 2013, **135**(31), 11603–11613.
27 A. Walcarius and L. Mercier, Mesoporous organosilica adsorbents: nanoengineered materials for removal of organic and inorganic pollutants, *J. Mater. Chem.*, 2010, **20**(22), 4478–4511.
28 B.-S. Lee, *et al.*, Synthesis of metal ion–histidine complex functionalized mesoporous silica nanocatalysts for enhanced light-free tooth bleaching, *Acta Biomater.*, 2011, **7**(5), 2276–2284.
29 R. A. Graff, T. M. Swanson and M. S. Strano, Synthesis of Nickel− Nitrilotriacetic Acid Coupled Single-Walled Carbon Nanotubes for Directed Self-Assembly with Polyhistidine-Tagged Proteins, *Chem. Mater.*, 2008, **20**(5), 1824–1829.
30 J. Kim, *et al.*, Ni–nitrilotriacetic acid-modified quantum dots as a site-specific labeling agent of histidine-tagged proteins in live cells, *Chem. Commun.*, 2008, (16), 1910–1912.
31 H. Gu, *et al.*, Biofunctional magnetic nanoparticles for protein separation and pathogen detection, *Chem. Commun.*, 2006, (9), 941–949.
32 W. Liu, L. Wang and R. Jiang, Specific enzyme immobilization approaches and their application with nanomaterials, *Top. Catal.*, 2012, **55**(16–18), 1146–1156.
33 L. Wang, *et al.*, Activity and stability comparison of immobilized NADH oxidase on multi-walled carbon nanotubes, carbon nanospheres, and single-walled carbon nanotubes, *J. Mol. Catal. B: Enzym.*, 2011, **69**(3), 120–126.
34 T. Sedaghat, *et al.*, Binuclear organotin (IV) complexes with adipic dihydrazones: Synthesis, spectral characterization, crystal structures and antibacterial activity, *J. Organomet. Chem.*, 2013, **737**, 26–31.
35 Y. Wang, *et al.*, Endosomolytic and Tumor-Penetrating Mesoporous Silica Nanoparticles for siRNA/miRNA Combination Cancer Therapy, *ACS Appl. Mater. Interfaces*, 2020, **12**(4), 4308–4322.
36 S. Sindhwani, *et al.*, The Entry of Nanoparticles into Solid Tumours, *Nat. Mater.*, 2020, **19**, 566.
37 J. Li, *et al.*, Reactive oxygen species-sensitive thioketal-linked mesoporous silica nanoparticles as drug carrier for effective antibacterial activity, *Mater. Des.*, 2020, **195**, 109021.
38 Z. Zhou, *et al.*, Gsh Depletion Liposome Adjuvant for Augmenting the Photothermal Immunotherapy of Breast Cancer, *Sci. Adv.*, 2020, **6**, eabc4373.
39 R. K. Kankala, *et al.*, Nanoarchitectured Structure and Surface Biofunctionality of Mesoporous Silica Nanoparticles, *Adv. Mater.*, 2020, **32**(23), 1907035.
40 T. Su, *et al.*, Sting Activation in Cancer Immunotherapy, *Theranostics*, 2019, **9**, 7759.
41 P. Barata, A. K. Sood and D. S. Hong, RNA-Targeted Therapeutics in Cancer Clinical Trials: Current Status and Future Directions, *Cancer Treat. Rev.*, 2016, **50**, 35.
42 Z. Li, *et al.*, Mesoporous Silica Nanoparticles with pH-Sensitive Nanovalves for Delivery of Moxifloxacin Provide Improved Treatment of Lethal Pneumonic Tularemia, *ACS Nano*, 2015, **9**, 10778.
43 J. Finlay, *et al.*, Mesoporous Silica Nanoparticle Delivery of Chemically Modified siRNA against TWIST1 Leads to Reduced Tumor Burden, *Nanomedicine*, 2015, **11**, 1657.
44 T. M. Guardado-Alvarez, M. M. Russell and J. I. Zink, Nanovalve Activation by Surface-Attached Photoacids, *Chem. Commun.*, 2014, **50**, 8388.
45 D. Tarn, *et al.*, A Reversible Light-Operated Nanovalve on Mesoporous Silica Nanoparticles, *Nanoscale*, 2014, **6**, 3335.
46 P. N. Durfee, *et al.*, Mesoporous Silica Nanoparticle-Supported Lipid Bilayers (Protocells) for Active Targeting and Delivery to Individual Leukemia Cells, *ACS Nano*, 2016, **10**, 8325.
47 S. Wilhelm, *et al.*, Analysis of Nanoparticle Delivery to Tumours, *Nat. Rev. Mater.*, 2016, **1**, 16014.
48 C. M. Roberts, *et al.*, Nanoparticle Delivery of siRNA against TWIST to Reduce Drug Resistance and Tumor Growth in Ovarian Cancer Models, *Nanomedicine*, 2017, **13**, 965.
49 S. L. Ginn, *et al.*, Gene Therapy Clinical Trials Worldwide to 2017: An Update, *J. Gene Med.*, 2018, **20**, e3015.
50 Z. A. Chen, *et al.*, Critical Features for Mesoporous Silica Nanoparticles Encapsulated into Erythrocytes, *ACS Appl. Mater. Interfaces*, 2019, **11**, 4790.
51 N. Cheng, *et al.*, A Nanoparticle-Incorporated Sting Activator Enhances Antitumor Immunity in Pd-L1-Insensitive Models of Triple-Negative Breast Cancer, *JCI Insight*, 2018, **3**, e120638.
52 L. Tahmasbi, T. Sedaghat, H. Motamedi and M. Kooti, Mesoporous silica nanoparticles supported copper(II) and nickel(II) Schiff base complexes: Synthesis, characterization, antibacterial activity and enzyme immobilization, *J. Solid State Chem.*, 2018, **258**, 517–525.
53 J. Li, *et al.*, Synthesis, amino-functionalization of mesoporous silica and its adsorption of Cr(VI), *J. Colloid Interface Sci.*, 2008, **318**(2), 309–314.
54 M. M. Bhadbhade and D. Srinivas, Effects on molecular association, chelate conformation, and reactivity toward substitution in copper Cu(5-X-salen) complexes, salen2- = *N*,*N*′-ethylenebis(salicylidenaminato), X = H, CH_3O, and Cl: synthesis, x-ray structures, and EPR investigations. [Erratum to document cited in CA119(26):285036b], *Inorg. Chem.*, 1993, **32**(26), 6122–6130.
55 D. Tang, *et al.*, Transition metal complexes on mesoporous silica nanoparticles as highly efficient catalysts for epoxidation of styrene, *J. Colloid Interface Sci.*, 2011, **356**(1), 262–266.
56 L. Tahmasbi, *et al.*, Mesoporous silica nanoparticles supported copper(II) and nickel(II) Schiff base complexes: Synthesis, characterization, antibacterial activity and enzyme immobilization, *J. Solid State Chem.*, 2018, **258**, 517–525.
57 K. Letchmanan, *et al.*, Mechanical properties and antibiotic release characteristics of poly(methyl methacrylate)-based bone cement formulated with mesoporous silica nanoparticles, *J. Mech. Behav. Biomed. Mater.*, 2017, **72**, 163–170.
58 L. Yang, *et al.*, One-pot synthesis of aldehyde-functionalized mesoporous silica-Fe_3O_4 nanocomposites for immobilization of penicillin G acylase, *Microporous Mesoporous Mater.*, 2014, **197**, 1–7.

59 W. Liu, L. Wang and R. Jiang, Specific Enzyme Immobilization Approaches and Their Application with Nanomaterials, *Top. Catal.*, 2012, **55**(16), 1146–1156.
60 X. Ma and S. Sánchez, Bio-catalytic mesoporous Janus nanomotors powered by catalase enzyme, *Tetrahedron*, 2017, **73**(33), 4883–4886.
61 D. N. Tran and K. J. Balkus, Perspective of Recent Progress in Immobilization of Enzymes, *ACS Catal.*, 2011, **1**(8), 956–968.
62 R. A. Sheldon, Enzyme Immobilization: The Quest for Optimum Performance, *Adv. Synth. Catal.*, 2007, **349**(8–9), 1289–1307.